J Mater Sci (2011) 46:372–384
DOI 10.1007/s10853-010-4846-0

A generalised three-dimensional tethered-nodule model for auxetic materials

N. Gaspar · C. W. Smith · A. Alderson · J. N. Grima · K. E. Evans

Received: 8 May 2010 / Accepted: 16 August 2010 / Published online: 31 August 2010

Abstract Models for the nano/micro-structural deformation and mechanical properties of auxetic materials (i.e. materials with a negative Poisson's ratio) have been previously developed. However, most of these models have been two-dimensional, were usually designed specifically to describe some particular class of auxetic materials, and generally only described the behaviour of one particular plane whilst completely ignoring the out-of-plane behaviour of the material. A three-dimensional model has been developed which can be applied to several classes of auxetic materials, including microporous expanded polymers such as e-PTFE, e-UHMWPE and e-PA, body-centered cubic metals and foams. It is generalised that its underlying structure is not specific to a lengthscale or material as the previous list shows. The new model offers a better insight into the underlying principles behind the observed auxetic behaviour and offers a significant improvement in the agreement of the models with existing experimental data. It is shown that there are geometric limitations to the number of planes that can simultaneously display auxetic behaviour. This has ramifications on the design of ordered auxetic materials.

N. Gaspar (✉)
AWE plc, Aldermaston, Reading RG7 4PR, UK
e-mail: neil@ngaspar.info

C. W. Smith · K. E. Evans
School of Engineering, Computing and Mathematics,
University of Exeter, North Park Road, Exeter EX4 4QF, UK
e-mail: c.w.smith@exeter.ac.uk

K. E. Evans
e-mail: k.e.evans@exeter.ac.uk

A. Alderson
Centre for Materials Research & Innovation,
University of Bolton, Deane Road, Bolton BL3 5AB, UK
e-mail: a.alderson@bolton.ac.uk

J. N. Grima
Department of Chemistry, Faculty of Science,
University of Malta, Msida, MSD 2080, Malta
e-mail: joseph.grima@um.edu.mt

Introduction

Materials with a negative Poisson's ratio (auxetic materials) have the unusual property of becoming wider when stretched and narrower when compressed [13]. This unusual mechanical property gives several beneficial effects such as increased shear stiffness, increased plane strain fracture toughness and increased indentation resistance [6], improvement of the dielectric properties of honeycombs [30], use for self-adaptive vibrational damping and auxetic molecular membranes for MEMS applications [11].

Negative Poisson's ratios have been discovered or predicted in a number of materials such as foams [23], microporous polymers [5, 6] [7], metals [8], and zeolites [21]. It arises from a combination of (i) particular geometric features in the micro or nanostructure of the materials, and, (ii) the deformation mechanisms. An understanding of the mechanisms giving rise to auxetic behaviour and the ability to predict mechanical properties is required for full exploitation of these materials. Several geometries and mechanisms have been used to explain the auxetic effect in these classes of materials, for example, auxetic foams have been commonly modelled through re-entrant cellular structures in 2D [19, 26] and also 3D [31], a number of predicted auxetic zeolites have been modelled in terms of rotating squares [20], whilst microporous polymers such as expanded polytetrafluoroethylene (ex-PTFE) have been explained in terms of elliptic-shaped nodules interconnected by fibrils where

proposed deformation mechanisms include rotating nodules and fibril hinging, subsequently fibril hinging and stretching [3, 28], [2, 4] and most recently, concurrent fibril hinging and stretching [1, 16].

All of these models are based on simple two dimensional models and hence they cannot simultaneously predict the Poisson's ratio for all three orthogonal planes. It is also clear that in some instances two dimensional models ignore three dimensional effects. In view of this, we propose a new three dimensional model based upon the two-dimensional, concurrent fibril hinging and stretching model for microporous polymers, in an attempt to derive a single generalised model that can be applied to several classes of materials including microporous polymers, porous materials with body centred cubic symmetry and foams.

The model

This new model is based on a periodic structure made up of tetragonal nodules of size (a, b, c) interconnected by rod-shaped elements of equal length ℓ shown in Fig. 1. The tetragonal unit cell contains two nodules arranged as in BCC form (i.e. one at the centre of the cell, and one in each corner) and eight rods arranged so that each of the eight vertices of the central nodule connects to the nearest vertex of an adjacent corner nodule as detailed in Fig. 2. The unit cell has three mutually orthogonal planes of symmetry perpendicular to the Cartesian axes and intersecting at the centre of the unit cell. This means that the eight rods in the unit cell can be treated as mirror images of a single rod, and referring to Fig. 2, we shall assume that the angular orientation of the rods can be described in terms of the angles ϕ and θ, where ϕ is the angle between the rods and the x_3 direction and θ is the angle that the image of the rod in the x_1–x_2 plane makes with the x_1 direction.

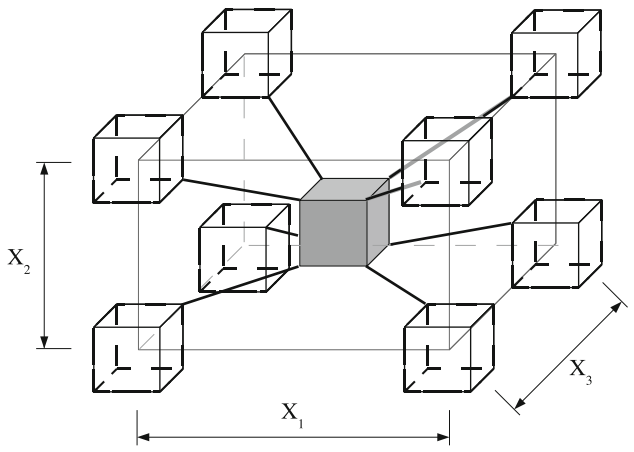

Fig. 1 Central nodule connected to eight others via corner fibrils

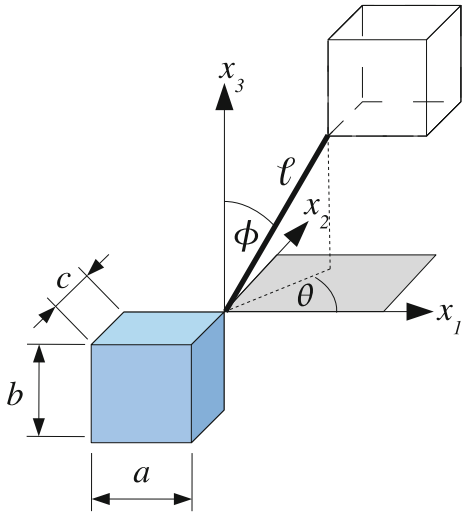

Fig. 2 Central nodule connected to eight others via corner fibrils

The projections of the unit cell in the x_i directions are given by:

$$X_1 = 2[a + \ell \cos\theta \sin\phi], \tag{1}$$

$$X_2 = 2[b + \ell \sin\theta \sin\phi], \tag{2}$$

$$X_3 = 2[c + \ell \cos\phi], \tag{3}$$

which naturally reduce to cubic symmetry when $X_1 = X_2 = X_3$.

Simple geometric constraints on θ and ϕ are:

$$-180^\circ \le \theta \le 180^\circ \text{ for } 0^\circ \le \phi \le 90^\circ \text{or} \tag{4}$$

$$-180^\circ \le \theta \le 90^\circ \text{ for } 90^\circ \le \phi \le 180^\circ \tag{5}$$

More complicated geometric constraints would prevent nodules and fibrils passing through each other. To do this the constraint would have to consider the relative size of the fibril lengths with the nodule thickness.

It shall be assumed that the model structure deforms through hinging and stretching of the rods, i.e. by changes in the geometric parameters ϕ, θ and ℓ such that stresses in the x_i directions will conserve the symmetry of the unit cell. It has been demonstrated previously that flexure of the rods produces the same behaviour as hinging and so can be considered as equivalent to or part of the hinging mechanism. A further assumption is that the deformation mechanisms work identically under compression or tension.

A final detail needed to arrange the mechanics is to write down the how a force on the fibril is projected into the directions of ℓ, θ and ϕ. This is done by inspection of Fig. 2 and the results below.

$$f_1 \cos\theta \sin\phi = f_\ell \quad f_2 \sin\theta \sin\phi = f_\ell \quad f_3 \cos\phi = f_\ell \tag{6}$$

$$f_1 \sin\theta = f_\theta \quad f_2 \cos\theta = f_\theta \tag{7}$$

$$f_1 \cos\theta \cos\phi = f_\phi \quad f_2 \sin\theta \cos\phi = f_\phi \quad f_3 \sin\phi = -f_\phi \tag{8}$$

Idealised single-mode deformations

Methodology

A common approach to developing a micromechanic formulation of such a microstructure is given by Love [25] and involves the products of branch vectors and their forces. This is often used in the granular mechanics community by for example Gaspar and Koenders [14]. Another approach is the use of an energy function whose derivatives return the imposed strain. In this work it is desired to examine the effect of changing the geometric and material parameters. Therefore, an approach is used that leads to simple explicit relations between bulk mechanical properties such as Poisson's ratio and the constitutive model parameters. While certain aspects of this approach are not elegant, as will be discussed later, it does give a clear ability to fit measured data and to discuss the relative impact of different parameters.

In the generalised scenario, the six geometric parameters may vary concurrently, that is, the size of the unit cell will be a function of the six parameters a, b, c, ϕ, θ and ℓ, i.e. $X_i = X_i(a, b, c, \phi, \theta, \ell)$. However, we shall first consider a simplified scenario where the structure is only allowed to deform through changes in one of ϕ, θ or ℓ at a time (idealised single-mode deformations). The nodule is assumed non-deformable at this stage so a, b and c will remain constant. The two hinging modes where ϕ or θ change correspond to tangential interactions and the stretching mode where ℓ changes corresponds to normal interactions with respect to the central nodule. A fully generalised model would include deformation and rotation of the nodules. These are ignored, firstly to keep the problem tractable and secondly to model materials that are dominated by the deformation of connective fibrils. An example of geometry that this does not model is the rotating squares structure by Grima et al. [20], which would be arrived at if $\ell = 0$ and nodule rotation was allowed.

Central to these models is the geometry construction of the unit cell, shown in Figs. 1 and 2. To form an incremental model for the relationship between stress and strain according to the cellular structure, the following methodology is used.

1. The lengths of the cell are described already in Eqs. 1–3 as some function of the internal geometric parameters.

$$X_i = F^{(1)}(\theta, \phi, \ell, a, b, c), \tag{9}$$

where the subscript i varies over the three axis. Their partial derivatives with respect to deformation variables are also required:

$$\frac{\partial X_i}{\partial \Lambda} = F^{(2)}(\theta, \phi, \ell, a, b, c), \tag{10}$$

where Λ takes θ, ϕ or ℓ as one of three independent deformation variables and $F^{(2)}$ is some set of algebraic functions.

2. The strain increment is defined from the increment of lengths of cell sides.

$$\mathrm{d}\epsilon_i = \frac{\mathrm{dX_i}}{X_i} = \frac{\partial X_i}{\partial \Lambda}\frac{\mathrm{d}\Lambda}{X_i} = F^{(4)}(\theta, \phi, \ell, a, b, c, d\Lambda). \tag{11}$$

Following in the same manner, the symmetrical shear strain is defined by

$$\mathrm{d}\eta_{(ij)} = \frac{1}{2}\left(\frac{\mathrm{dX_i}}{X_j} + \frac{\mathrm{dX_j}}{X_i}\right). \tag{12}$$

3. Relating stress and strain increments requires the internal deformation mechanism that algebraically relate force increment $\mathrm{d}f_\Lambda$ with $\mathrm{d}\Lambda$ in step 2). For this elastic heart of the model, linear elasticity is chosen. More sophisticated models could be inserted, especially bending beam interactions, but the focus of this work is the geometry dependence of the elastic moduli. As long as deformations are small then linear elasticity will suffice. These elastic models are:

$$\mathrm{d}f_\ell = k_\ell \mathrm{d}\ell, \tag{13}$$

$$\mathrm{d}f_\theta \ell = k_\theta \mathrm{d}\theta, \tag{14}$$

$$\mathrm{d}f_\phi \ell = k_\phi \mathrm{d}\phi. \tag{15}$$

In the case of the deformation of angles θ and ϕ, the force moments $\mathrm{d}f_\theta\ell$ and $\mathrm{d}f_\phi\ell$ are defined to be acting in the plane of the angular change $\mathrm{d}\theta$ or $\mathrm{d}\phi$. The details of which are contained within the expressions of Eq. 16.

4. The stress increment is described as a function of internal geometric parameters and the force increment f_i. Normal stress represented by σ and shear stress by τ.

$$\mathrm{d}\sigma_i = F^{(3)}(\theta, \phi, \ell, a, b, c, \mathrm{d}f_\Lambda), \tag{16}$$

where subscript Λ varies over the three deforming variable θ, ϕ or ℓ and subscript i varies over the Cartesian axes.

5. Finally, elastic moduli, Young's modulus, Poisson's ratio and shear modulus, respectively, are calculated as follows:

$$E_i = \frac{\mathrm{d}\sigma_\mathrm{i}}{\mathrm{d}\epsilon_j}, \tag{17}$$

$$v_{ij} = -\frac{\mathrm{d}\epsilon_j}{\mathrm{d}\epsilon_i}, \tag{18}$$

$$\mu_{ij} = \frac{\tau_{ij}}{\eta_{ij}}. \tag{19}$$

Idealised stretching model

We shall first consider the scenario where the structure is allowed to deform solely through stretching implying the use of Eq. 13 and the assumption $k_\ell \ll k_\theta, k_\phi$. We start with the standard relationship between stress and strain recognising that there are 4 fibrils that contribute to the stress over a single face. Using the x_1 axis as an example for the stress increments in Eq. 16: $\sigma_1 = 4\mathrm{d}f_1/X_2X_3$. We have Eqs. 6–8 to give $\mathrm{d}f_1$ in terms of the $\mathrm{d}f_\ell$. Replicating this example for all the stress components gives:

$$\mathrm{d}\sigma_1 = 4\frac{\mathrm{d}f_\ell}{\cos\theta\sin\phi X_2X_3}, \tag{20}$$

$$\mathrm{d}\sigma_2 = 4\frac{\mathrm{d}f_\ell}{\sin\theta\sin\phi X_1X_3}, \tag{21}$$

$$\mathrm{d}\sigma_3 = 4\frac{\mathrm{d}f_\ell}{\cos\phi X_1X_2}, \tag{22}$$

$$\mathrm{d}\tau_{12} = 4\frac{\mathrm{d}f_\ell}{\cos\theta\sin\phi X_1X_3}, \quad \mathrm{d}\tau_{13} = 4\frac{\mathrm{d}f_\ell}{\cos\theta\sin\phi X_1X_2}, \tag{23}$$

$$\mathrm{d}\tau_{21} = 4\frac{\mathrm{d}f_\ell}{\sin\theta\sin\phi X_2X_3}, \quad \mathrm{d}\tau_{23} = 4\frac{\mathrm{d}f_\ell}{\sin\theta\sin\phi X_2X_1}, \tag{24}$$

$$\mathrm{d}\tau_{31} = 4\frac{\mathrm{d}f_\ell}{\cos\phi X_3X_2}, \quad \mathrm{d}\tau_{32} = 4\frac{\mathrm{d}f_\ell}{\cos\phi X_3X_1}. \tag{25}$$

For the strain increments we need first the partial derivatives of the unit cell size from Eq. 10.

$$\frac{\partial X_1}{\partial \ell} = 2\cos\theta\sin\phi, \tag{26}$$

$$\frac{\partial X_2}{\partial \ell} = 2\sin\theta\sin\phi, \tag{27}$$

$$\frac{\partial X_3}{\partial \ell} = 2\cos\phi. \tag{28}$$

Strain increments from Eqs. 11 and 12 with the deformation model included are therefore

$$\mathrm{d}\epsilon_1 = \frac{2\cos\theta\sin\phi}{k_\ell X_1}\mathrm{d}f_\ell, \tag{29}$$

$$\mathrm{d}\epsilon_2 = \frac{2\sin\theta\sin\phi}{k_\ell X_2}\mathrm{d}f_\ell, \tag{30}$$

$$\mathrm{d}\epsilon_3 = \frac{2\cos\phi}{k_\ell X_3}\mathrm{d}f_\ell, \tag{31}$$

$$\mathrm{d}\eta_{12} = \frac{X_2\cos\theta\sin\phi + X_1\sin\theta\sin\phi}{k_\ell X_1X_2}\mathrm{d}f_\ell, \tag{32}$$

$$\mathrm{d}\eta_{13} = \frac{X_3\cos\theta\sin\phi + X_1\cos\phi}{k_\ell X_1X_3}\mathrm{d}f_\ell, \tag{33}$$

$$\mathrm{d}\eta_{23} = \frac{X_3\sin\theta\sin\phi + X_2\cos\phi}{k_\ell X_2X_3}\mathrm{d}f_\ell. \tag{34}$$

We are now in a position to calculate the Young's modulus and Poisson's ratio from Eqs. 17 and 18.

Young's modulus and Poisson's ratio

In both the Young's modulus and the Poisson's ratio, the deformation $\mathrm{d}\ell$ naturally cancels out leaving only geometric parameters and, in the case of the Young's modulus, the force constant k_ℓ. The resulting equations are:

$$E_1^\ell = \frac{2k_\ell}{\cos^2\theta\sin^2\phi}\frac{X_1}{X_2X_3}, \tag{35}$$

$$E_2^\ell = \frac{2k_\ell}{\sin^2\theta\sin^2\phi}\frac{X_2}{X_1X_3}, \tag{36}$$

$$E_3^\ell = \frac{2k_\ell}{\cos^2\phi}\frac{X_3}{X_1X_2}, \tag{37}$$

$$v_{31}^\ell = \left(v_{13}^\ell\right)^{-1} = -\cos\theta\tan\phi\frac{X_3}{X_1}, \tag{38}$$

$$v_{12}^\ell = \left(v_{21}^\ell\right)^{-1} = -\tan\theta\frac{X_1}{X_2}, \tag{39}$$

$$v_{32}^\ell = \left(v_{23}^\ell\right)^{-1} = -\sin\theta\tan\phi\frac{X_3}{X_2}. \tag{40}$$

These expressions show that whilst all the geometric parameters a, b, c, ℓ, θ and ϕ play a role in the magnitude of the six on-axis Poisson's ratios, the sign of the six on-axis Poisson's ratios (i.e. the existence or otherwise of auxetic behaviour) will depend only on the orientation of the rods (i.e. on the geometric parameters θ and ϕ). As indicated in Fig. 3, the structure will be fully auxetic (i.e. all six Poisson's ratios are negative) when $0° \le \theta \le 90°$ and $0° \le \phi \le 90°$. Consideration of the constraints in Eqs. 4 and 5 marks one region as unphysical, with this nodule-fibril arrangement, the fibril is superimposed within the nodule. Were this region to be physically viable it would also be fully auxetic. The fully auxetic regime marked in Fig. 3 corresponds to the granular system by Bathurst and Rothenburg [9] and others whereby tangential interactions are constrained through a large stiffness and therefore normal interactions are favoured.

In the range of angles that does produce three negative Poisson's ratio simultaneously, the projection of the structure in the three x_i–x_j ($i, j = 1, 2, 3$) planes will not

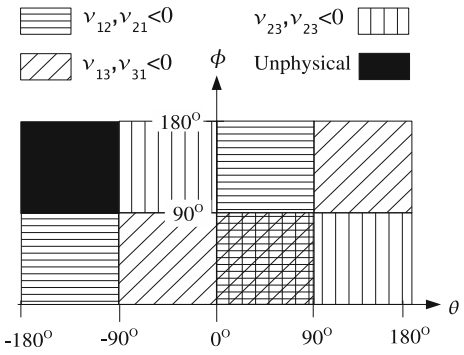

Fig. 3 Phase diagram showing regions of negative Poisson's ratio for fibril stretching only

contain any re-entrant geometries. To make the term "re-entrant" objective we refer to a periodic array of Fig. 1, whereby all fibrils in the first quadrant (as drawn in Fig. 1) are not re-entrant.

In the other combinations of ϕ and θ, auxetic behaviour is observed in only one of the three x_i–x_j ($i, j = 1, 2, 3$) planes at a time. The full phase diagram of the regions of negative Poisson's ratio for all three axes is shown in Fig. 3.

Shear modulus

A problem arises with the shear modulus. For the majority of cases, it is not possible to evaluate a shear modulus for this general 3D model. In the general case, reasons why the shear modulus may not be evaluated are as follows:

1. Symmetry locking: this model places the unit cell in a repeating medium but many deformations break this symmetry. In effect the deformation will be locked as some elements are forced into two conflicting deformations simultaneously. For instance, when $\phi = \theta = 45°$ and deformation is by fibril stretching, shear deformation on the unit cell will cause some fibrils to extend and some to contract. If this is placed in the appropriate repeating pattern then all fibrils are required to contract and all extend simultaneously.
2. Deformation in a particular plane does not exist by a choice of parameters: the definition of, for example, θ and its deformation does not alter lengths in the x_3 dimension. Hence any shear strain $d\eta_{i3}$ due to θ bending is zero and the associated shear modulus not-defined (infinite).
3. Shear strain does not exist: consider an applied shear in the x_1–x_2 plane and deformation due to θ bending, see Fig. 4. Considering the central nodule and just four of its connected nodules in this plane, the applied shearing will cause either four angles to increase or two angles to increase and two to decrease depending on boundary conditions. Looking at Fig. 4 it can be seen for the former there is no shear deformation with these material axis. The latter involves a complicated folding of the structure that contains a combination of shear and normal deformation. Either way no shear strain is obtained.

The specific case of fibrils that do not bend turns the material into one described by Bathurst and Rothenburg [10, 17]. Here the isotropic limit of $\nu = -1$ is reached and the material only deforms though volume change; there is no shear deformation or in other words the shear modulus is very much bigger than the bulk modulus.

A limited number of shear moduli can be evaluated for the stretching model when the angles in the model approximate the geometry to 2D; they are when $\phi = 90°$ or $\theta = 0°$ or $\theta = 90°$.

By allowing concurrent deformation there are now viable shear modes for deformation of the unit cell. There is, however, a significant problem to calculating the on-axis shear, *to wit* quantifying the relative stretching and bending that is used. The obvious technique is to minimise the combined elastic energy from stretching and bending for any particular shear deformation. However, the geometry renders this algebraically intractable and solutions are not attempted here.

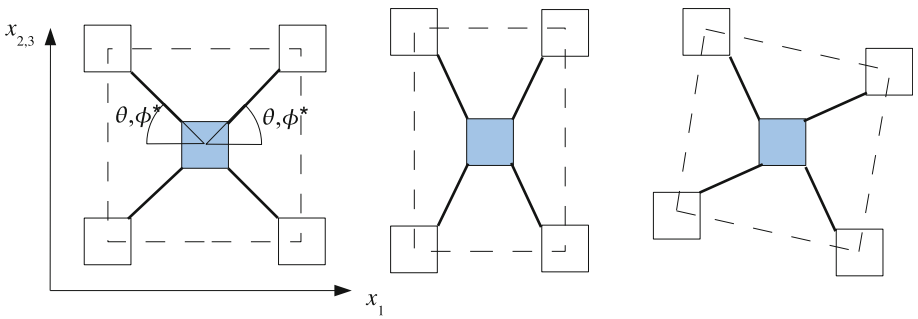

Fig. 4 A projection in the x_1–x_2 axis or x_1–x_3 axis with angle θ or projected angle ϕ^* marked on the *left* and on the *right*. Reference cell (*left*) and two different symmetry cases (*middle* and *right*) for deformation of the marked angle. In the first case (*middle*), the *left* and *right* angles change together. In the second case (*right*), the change of *left* and *right* angles have opposite signs

The idealised ϕ hinging model

Let us now consider the scenario where the structure is allowed to deform solely through hinging in angle ϕ. Our choice of deformation then uses Eq. 15. For the record, the stress increments are

$$\begin{aligned} \mathrm{d}\sigma_1 &= \frac{4\mathrm{d}f_\phi}{\cos\theta\cos\phi X_2X_3}, \quad \mathrm{d}\tau_{12} = \frac{4\mathrm{d}f_\phi}{\cos\theta\cos\phi X_1X_3}, \\ \mathrm{d}\tau_{13} &= \frac{4\mathrm{d}f_\phi}{\cos\theta\cos\phi X_1X_2}, \end{aligned} \tag{41}$$

$$\begin{aligned} \mathrm{d}\sigma_2 &= \frac{4\mathrm{d}f_\phi}{\sin\theta\cos\phi X_1X_3}, \quad \mathrm{d}\tau_{21} = \frac{4\mathrm{d}f_\phi}{\sin\theta\cos\phi X_2X_3}, \\ \mathrm{d}\tau_{23} &= \frac{4\mathrm{d}f_\phi}{\sin\theta\cos\phi X_2X_1}, \end{aligned} \tag{42}$$

$$\begin{aligned} \mathrm{d}\sigma_3 &= \frac{-4\mathrm{d}f_\phi}{\sin\phi X_1X_2}, \quad \mathrm{d}\tau_{31} = \frac{4\mathrm{d}f_\phi}{\sin\phi X_3X_2}, \\ \mathrm{d}\tau_{32} &= \frac{4\mathrm{d}f_\phi}{\sin\phi X_3X_1}, \end{aligned} \tag{43}$$

and the strain increments are

$$\begin{aligned} \mathrm{d}\epsilon_1 &= \frac{2\ell^2\cos\theta\cos\phi}{k_\phi X_1}\mathrm{d}f_\phi, \\ \mathrm{d}\eta_{12} &= \frac{\ell^2(X_2\cos\theta\cos\phi + X_1\sin\theta\cos\phi)}{k_\phi X_1X_2}\mathrm{d}f_\phi, \end{aligned} \tag{44}$$

$$\begin{aligned} \mathrm{d}\epsilon_2 &= \frac{2\ell^2\sin\theta\cos\phi}{k_\phi X_2}\mathrm{d}f_\phi, \\ \mathrm{d}\eta_{13} &= \frac{\ell^2(X_3\cos\theta\cos\phi - X_1\sin\phi)}{k_\phi X_1X_3}\mathrm{d}f_\phi, \end{aligned} \tag{45}$$

$$\begin{aligned} \mathrm{d}\epsilon_3 &= \frac{-2\ell^2\sin\phi}{k_\phi X_3}\mathrm{d}f_\phi, \\ \mathrm{d}\eta_{23} &= \frac{\ell^2(X_3\sin\theta\cos\phi - X_2\sin\phi)}{k_\phi X_2X_3}\mathrm{d}f_\phi. \end{aligned} \tag{46}$$

Accordingly, the elastic moduli are

$$\begin{aligned} E_1^\phi &= \frac{2k_\phi}{\ell^2\cos^2\theta\cos^2\phi}\frac{X_1}{X_2X_3}, \\ v_{12}^\phi &= \left(v_{21}^\phi\right)^{-1} = -\tan\theta\frac{X_1}{X_2}, \end{aligned} \tag{47}$$

$$\begin{aligned} E_2^\phi &= \frac{2k_\phi}{\ell^2\sin^2\theta\cos^2\phi}\frac{X_2}{X_1X_3}, \\ v_{31}^\phi &= \left(v_{13}^\phi\right)^{-1} = \cos\theta\cot\phi\frac{X_3}{X_1}, \end{aligned} \tag{48}$$

$$E_3^\phi = \frac{2k_\phi}{\ell^2\sin^2\phi}\frac{X_3}{X_1X_2}, \quad v_{32}^\phi = \left(v_{23}^\phi\right)^{-1} = \sin\theta\cot\phi\frac{X_3}{X_2}. \tag{49}$$

There are no cases where shear is an allowable deformation mode for ϕ bending. In all cases the regular array suffers symmetry locking.

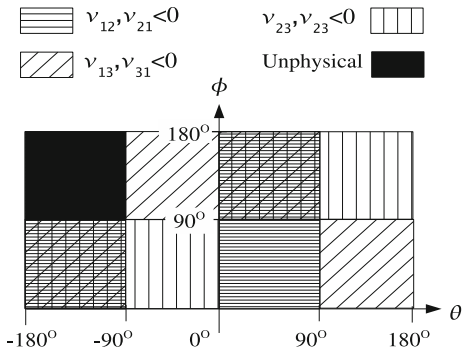

Fig. 5 Phase diagram showing regions of negative Poisson's ratio for ϕ-bending only

As in the case of idealised stretching, the expressions for the Poisson's ratio for the idealised ϕ hinging model show that the sign of the six Poisson's ratios will depend only on particular values of the geometric parameters θ and ϕ, although the geometric parameters a, b, c, ℓ, θ and ϕ determine their magnitude. The phase diagram for the regions of θ and ϕ that are negative is shown in Fig. 5. Notably, the region for all three axes to display a negative Poisson's ratio does not intersect with that for idealised stretching. This will have ramifications when concurrent deformation modes are considered.

The idealised θ hinging model

The third component to idealised single-mode deformation is hinging in angle θ using Eq. 14. The location of θ in the x_1–x_2 plane means that there are no out of plane stresses or strains (also force or displacements) of the unit cell associated with the deformation $\mathrm{d}\theta$. Hence $\mathrm{d}\sigma_3$, $\mathrm{d}\varepsilon_3$ and associated shear components cannot be evaluated. For the record, the stress increments are

$$\begin{aligned} \mathrm{d}\sigma_1 &= \frac{-4\mathrm{d}f_\theta}{\sin\theta X_2X_3}, \quad \mathrm{d}\tau_{12} = \frac{-4\mathrm{d}f_\theta}{\sin\theta\cos\phi X_1X_3}, \\ \mathrm{d}\tau_{13} &= \frac{-4\mathrm{d}f_\theta}{\sin\theta\cos\phi X_1X_2}, \end{aligned} \tag{50}$$

$$\begin{aligned} \mathrm{d}\sigma_2 &= \frac{4\mathrm{d}f_\theta}{\cos\theta X_1X_3}, \quad \mathrm{d}\tau_{21} = \frac{4\mathrm{d}f_\theta}{\cos\theta\cos\phi X_2X_3}, \\ \mathrm{d}\tau_{23} &= \frac{4\mathrm{d}f_\theta}{\cos\theta\cos\phi X_2X_1}, \end{aligned} \tag{51}$$

and the strain increments are

$$\begin{aligned} \mathrm{d}\epsilon_1 &= \frac{-2\ell^2\sin\theta\sin\phi}{k_\theta X_1}\mathrm{d}f_\theta, \\ \mathrm{d}\eta_{12} &= \frac{\ell^2(X_2\sin\theta\cos\phi + X_1\sin\theta\sin\phi)}{k_\theta X_1X_2}\mathrm{d}f_\theta, \end{aligned} \tag{52}$$

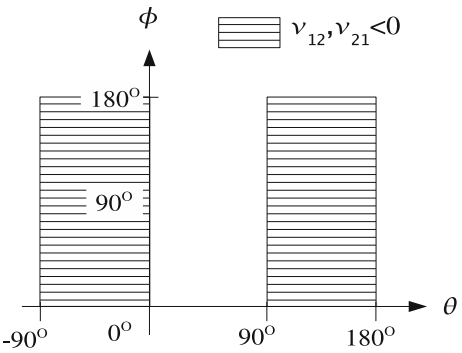

Fig. 6 Phase diagram showing regions of negative Poisson's ratio for θ deformation only

$$\mathrm{d}\epsilon_2 = \frac{2\ell^2 \cos\theta \sin\phi}{k_\theta X_2}\mathrm{d}f_\theta, \quad \mathrm{d}\eta_{13} = \frac{\ell^2 (X_3 \sin\theta \cos\phi)}{k_\ell X_1 X_3}\mathrm{d}f_\phi, \tag{53}$$

$$\mathrm{d}\eta_{23} = \frac{\ell^2 \sin\theta \sin\phi}{k_\ell X_2}\mathrm{d}f_\phi. \tag{54}$$

The elastic moduli that do exist are

$$E_1^\phi = \frac{2k_\theta}{\ell^2 \sin^2\theta \sin\phi}\frac{X_1}{X_2 X_3}, \quad \nu_{12}^\phi = \left(\nu_{21}^\phi\right)^{-1} = \cot\theta \frac{X_1}{X_2}, \tag{55}$$

$$E_2^\phi = \frac{2k_\theta}{\ell^2 \cos^2\theta \sin\phi}\frac{X_2}{X_1 X_3}. \tag{56}$$

There are no cases where shear is an allowable deformation. In all cases the regular array locks.

As with the previous two deformation mechanisms, the regions in the ϕ–θ space that produce a negative Poisson's ratio is mapped in Fig. 6.

Results

We now consider some physically reasonable examples relating to earlier work to demonstrate the results of these equations. Previous work [5–7], on microporous polyethylene demonstrated a microstructure to which this model can be applied. The previous model used and the equivalent variables for this model are shown in Fig. 7.

Alderson et al. [7] report measured values of engineering strain and Poisson's ratio and compare them with a 2D model that is equivalent to the θ bending of this model. Their model predicts the Poisson's ratio to be

$$\nu_{rz} = -\frac{\cos\alpha(A + L\cos\alpha)}{\sin\alpha(B - L\sin\alpha),} \tag{57}$$

and the model in this paper predicts

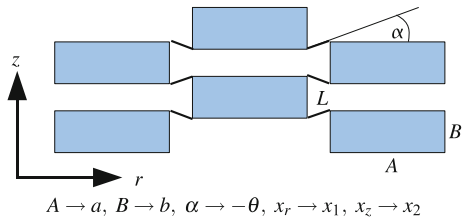

Fig. 7 The representative 2D geometry of UHMWPE as used by Alderson et al. [7] and the mapping to the variables used here. Results presume the material starts in its full expanded state which implies $\theta = 0$. In this model the fully expanded state also implies a value of $\phi = \pi/2$ which otherwise has no analogy in Alderson et al.'s 2D model. Other geometric parameters are $a = b = 20\ell$

$$\nu_{12} = \frac{\cos\theta(a + \ell\cos\theta\sin\phi)}{\sin\theta(b + \ell\sin\theta\sin\phi)}. \tag{58}$$

Likewise, the engineering strain is calculated by Alderson et al. to be

$$\epsilon_r = \frac{L(\cos\alpha - 1)}{A + L}, \tag{59}$$

and the model in this paper predicts the equivalent equation:

$$\epsilon_1 = \frac{\ell\sin\phi(\cos\theta - 1)}{a + \ell\sin\phi}. \tag{60}$$

The mathematical equivalence between the two models is evident for both engineering strain and Poisson's ratio when the third dimension is projected flat, i.e. $L = \ell\sin\phi$ and the difference in sign of θ and ϕ is allowed according to the mapping of variables in Fig. 7.

Alderson et al. [7] show a correlation between the measured data and their model. In this work we extend the comparison by fitting all three deformation mechanisms to their measured data. This is shown in Fig. 8 where values for ℓ, θ and ϕ have been chosen to best fit some portion of the graph. It can be seen that θ deformation and ϕ deformation seem to match different portions of the data, however, there can be no transition from one to the other as they represent quite different locations of the fibril about the nodule. Deformation by stretching fails to match any deformation as it is unable to provide a sufficiently large engineering strain. Single mode deformation does not fit the measured data well.

Concurrent deformations

Methodology

A force applied to the face of the unit cell is transmitted through the nodules to the deforming fibrils. The fibrils

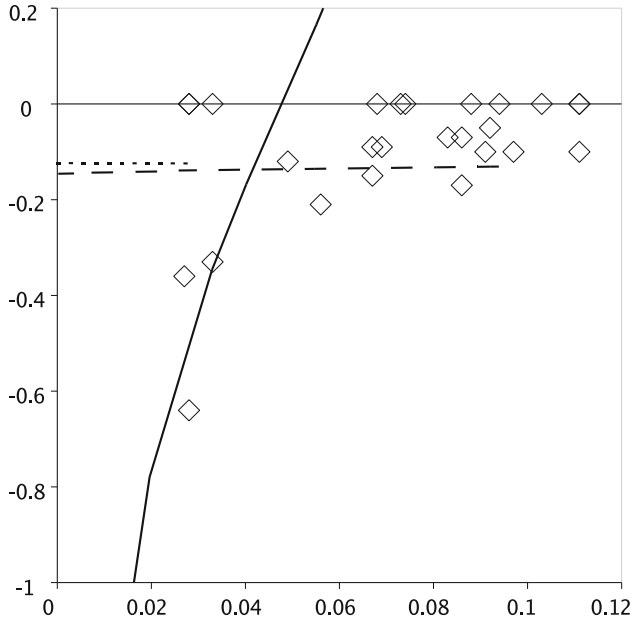

Fig. 8 Poisson's ratio against engineering strain for measured UHMWPE (*open diamond*), stretching deformation using $\ell = 1 \rightarrow 1.5$, $\theta = \pi/24$, $\phi = \pi/2$ (*dashed line*), ϕ deformation using $\phi = \pi/2 \rightarrow -\pi/2$, $\ell = 1$, $\theta = \pi/24$ (*dotted line*) and θ deformation using $\theta = 0 \rightarrow -\pi/2$, $\ell = 1$, $\phi = \pi/2$ (*solid line*)

have three deforming components: length, azimuth and elevation, whose combined deformation sums to the total deformation of the fibril. Concurrent deformation will therefore be treated as three elastic bodies in coupled series each experiencing the same force. The expectation is then for a more compliant material. Noting that it is the same force acting on all three elastic elements of a single fibril, relationships between the force components of the three mechanisms can be obtained. This will be used to obtain the relative amounts of deformation by the three mechanisms.

1. Forces acting on the unit cell in the x_1 direction are taken from Eqs. 20, 41 and 50.

$$\mathrm{d}\sigma_1^c = \mathrm{d}\sigma_1^\ell = \mathrm{d}\sigma_1^\phi = \mathrm{d}\sigma_1^\theta \tag{61}$$

$$\frac{\mathrm{df}_\ell}{\cos\theta\sin\phi} = \frac{\mathrm{df}_\phi}{\cos\theta\cos\phi} = \frac{-\mathrm{df}_\theta}{\sin\theta} \tag{62}$$

hence

$$\frac{\mathrm{df}_\ell}{\mathrm{df}_\phi} = \tan\phi, \quad \frac{\mathrm{df}_\ell}{\mathrm{df}_\theta} = -\cot\theta\sin\phi, \quad \frac{\mathrm{df}_\phi}{\mathrm{df}_\theta} = -\cot\theta\cos\phi. \tag{63}$$

2. Forces acting on the unit cell in the x_2 direction are taken from Eqs. 21, 42 and 51.

$$\mathrm{d}\sigma_2^c = \mathrm{d}\sigma_2^\ell = \mathrm{d}\sigma_2^\phi = \mathrm{d}\sigma_2^\theta \tag{64}$$

$$\frac{\mathrm{df}_\ell}{\sin\theta\sin\phi} = \frac{\mathrm{df}_\phi}{\sin\theta\cos\phi} = \frac{\mathrm{df}_\theta}{\cos\theta} \tag{65}$$

hence

$$\frac{\mathrm{df}_\ell}{\mathrm{df}_\phi} = \tan\phi, \quad \frac{\mathrm{df}_\ell}{\mathrm{df}_\theta} = \tan\theta\sin\phi, \quad \frac{\mathrm{df}_\phi}{\mathrm{df}_\theta} = \tan\theta\cos\phi. \tag{66}$$

3. Forces acting on the unit cell in the x_3 direction are taken from Eqs. 22 and 43.

$$\mathrm{d}\sigma_3^c = \mathrm{d}\sigma_3^\ell = \mathrm{d}\sigma_3^\phi = \mathrm{d}\sigma_3^\theta \tag{67}$$

$$\frac{\mathrm{df}_\ell}{\cos\phi} = -\frac{\mathrm{df}_\phi}{\sin\phi}, \tag{68}$$

hence

$$\frac{\mathrm{df}_\ell}{\mathrm{df}_\phi} = -\cot\phi. \tag{69}$$

Strictly speaking, the strain due to concurrent deformation is expressed as

$$\mathrm{d}\epsilon_i = \frac{\mathrm{dX_i}}{X_i} = \frac{\partial X_i}{\partial\ell}\frac{\mathrm{d}\ell}{X_i} + \frac{\partial X_i}{\partial\phi}\frac{\mathrm{d}\phi}{X_i} + \frac{\partial X_i}{\partial\theta}\frac{\mathrm{d}\theta}{X_i} \tag{70}$$

$$\mathrm{d}\epsilon_i^c = \mathrm{d}\epsilon_i^\ell + \mathrm{d}\epsilon_i^\phi + \mathrm{d}\epsilon_i^\theta \tag{71}$$

In long hand these are

$$\mathrm{d}\epsilon_1 = \left(\frac{2\cos\theta\sin\phi}{X_1}\mathrm{d}\ell + \frac{2\ell\cos\theta\cos\phi}{X_1}\mathrm{d}\phi - \frac{2\ell\sin\theta\sin\phi}{X_1}\mathrm{d}\theta\right), \tag{72}$$

$$\mathrm{d}\epsilon_2 = \left(\frac{2\sin\theta\sin\phi}{X_2}\mathrm{d}\ell + \frac{2\ell\sin\theta\cos\phi}{X_2}\mathrm{d}\phi + \frac{2\ell\cos\theta\sin\phi}{X_2}\mathrm{d}\theta\right), \tag{73}$$

$$\mathrm{d}\epsilon_3 = \left(\frac{2\cos\phi}{X_3}\mathrm{d}\ell - \frac{2\ell\sin\phi}{X_3}\mathrm{d}\phi\right). \tag{74}$$

Each measure of strain above has a contribution from each of the three deformation mechanisms. An applied driving force will contribute to those deformation mechanisms according to Eqs. 63, 66 or 69 depending on whether the applied stress is in the x_1, x_2, or x_3 directions, respectively.

Young's modulus

For the Young's modulus an applied force in the x_1 direction as described by Eq. 63 is substituted into the concurrent $d\varepsilon_1$ deformation in Eq. 72, and so on for the x_2 and x_3 axis. Use is also made of the elastic kernel, Eqs. 13,

14 and 15. The final result is arbitrarily chosen to be in terms of the small increment of force df_ℓ.

$$d\epsilon_1 = \left(\frac{2\cos\theta\sin\phi}{k_\ell X_1} + \frac{2\ell^2\cos\theta\cos\phi\cot\phi}{k_\phi X_1} + \frac{2\ell^2\sin\theta\tan\theta}{k_\theta X_1}\right) df_\ell \tag{75}$$

$$d\epsilon_2 = \left(\frac{2\sin\theta\sin\phi}{k_\ell X_2} + \frac{2\ell^2\sin\theta\cos\phi\cot\phi}{k_\phi X_2} + \frac{2\ell^2\cos\theta\cot\theta}{k_\theta X_2}\right) df_\ell \tag{76}$$

$$d\epsilon_3 = \left(\frac{2\cos\phi}{k_\ell X_3} - \frac{2\ell^2\sin\phi\tan\phi}{k_\phi X_3}\right) df_\ell \tag{77}$$

The definition of the Young's modulus written out for this concurrent deformation is

$$\left(E_i^c\right)^{-1} = \frac{d\epsilon_i^\ell + d\epsilon_i^\phi + d\epsilon_i^\theta}{d\sigma_i^c}. \tag{78}$$

The Young's moduli for the combining all three deformation modes are, therefore, as follows

$$\left(E_1^c\right)^{-1} = \frac{\left(\frac{2\cos\theta\sin\phi}{k_\ell X_1} + \frac{2\ell^2\cos\theta\cos\phi\cot\phi}{k_\phi X_1} + \frac{2\ell^2\sin\theta\tan\theta}{k_\theta X_1}\right) df_\ell}{\frac{4df_\ell}{\cos\theta\sin\phi X_2 X_3}} \tag{79}$$

$$= \frac{X_2X_3}{2X_1}\left(\frac{\cos^2\theta\sin^2\phi}{k_\ell} + \frac{\ell^2\cos^2\theta\cos^2\phi}{k_\phi} + \frac{\ell^2\sin^2\theta\sin\phi}{k_\theta}\right), \tag{80}$$

$$\left(E_2^c\right)^{-1} = \frac{\left(\frac{2\sin\theta\sin\phi}{k_\ell X_2} + \frac{2\ell^2\sin\theta\cos\phi\cot\phi}{k_\phi X_2} + \frac{2\ell^2\cos\theta\cot\theta}{k_\theta X_2}\right) df_\ell}{\frac{4df_\ell}{\sin\theta\sin\phi X_1 X_3}} \tag{81}$$

$$= \frac{X_1X_3}{2X_2}\left(\frac{\sin^2\theta\sin^2\phi}{k_\ell} + \frac{\ell^2\sin^2\theta\cos^2\phi}{k_\phi} + \frac{\ell^2\cos^2\theta\sin\phi}{k_\theta}\right), \tag{82}$$

$$\left(E_3^c\right)^{-1} = \frac{\left(\frac{2\cos\phi}{k_\ell X_3} + \frac{2\ell^2\sin\phi\tan\phi}{k_\phi X_3}\right) df_\ell}{\frac{4df_\ell}{\cos\phi X_1 X_2}} \tag{83}$$

$$= \frac{X_1X_2}{2X_3}\left(\frac{\cos^2\phi}{k_\ell} + \frac{\ell^2\sin^2\phi}{k_\phi}\right). \tag{84}$$

Poisson's ratio

The Poisson's ratio is of course defined by

$$\nu_{ij} = -\frac{d\epsilon_j}{d\epsilon_i}, \tag{85}$$

where $d\varepsilon_i$ is the axis with the applied force. This is essential for choosing the correct equation of 63, 66 or 69 to substitute into the concurrent deformations in 72, 73 or 74.

The Poisson's ratios then simplify to

$$\nu_{12} = -\frac{d\epsilon_2}{d\epsilon_1} = -\frac{X_1}{X_2}\frac{\frac{\sin\theta\sin\phi}{k_\ell} + \frac{\ell^2\sin\theta\cos\phi\cot\phi}{k_\phi} - \frac{\ell^2\sin\theta}{k_\theta}}{\frac{\cos\theta\sin\phi}{k_\ell} + \frac{\ell^2\cos\theta\cos\phi\cot\phi}{k_\phi} + \frac{\ell^2\sin\theta\tan\theta}{k_\theta}}, \tag{86}$$

$$\nu_{13} = -\frac{d\epsilon_3}{d\epsilon_1} = -\frac{X_1}{X_3}\frac{\frac{\cos\phi}{k_\ell} - \frac{\ell^2\cos\phi}{k_\phi}}{\frac{\cos\theta\sin\phi}{k_\ell} + \frac{\ell^2\cos\theta\cot\phi\cos\phi}{k_\phi} + \frac{\ell^2\sin\theta\tan\theta}{k_\theta}}, \tag{87}$$

$$\nu_{23} = -\frac{d\epsilon_3}{d\epsilon_2} = -\frac{X_2}{X_3}\frac{\frac{\cos\phi}{k_\ell} - \frac{\ell^2\cos\phi}{k_\phi}}{\frac{\sin\theta\sin\phi}{k_\ell} + \frac{\ell^2\sin\theta\cos\phi\cot\phi}{k_\phi} + \frac{\ell^2\cos\theta\cot\theta}{k_\theta}}, \tag{88}$$

$$\nu_{21} = -\frac{d\epsilon_1}{d\epsilon_2} = -\frac{X_2}{X_1}\frac{\frac{\cos\theta\sin\phi}{k_\ell} + \frac{\ell^2\cos\theta\cot\phi\cos\phi}{k_\phi} - \frac{\ell^2\cos\theta}{k_\theta}}{\frac{\sin\theta\sin\phi}{k_\ell} + \frac{\ell^2\sin\theta\cos\phi\cot\phi}{k_\phi} + \frac{\ell^2\cos\theta\cot\theta}{k_\theta}}, \tag{89}$$

$$\nu_{31} = -\frac{d\epsilon_1}{d\epsilon_3} = -\frac{X_3}{X_1}\frac{\frac{\cos\theta\sin\phi}{k_\ell} - \frac{\ell^2\cos\theta\sin\phi}{k_\phi}}{\frac{\cos\phi}{k_\ell} + \frac{\ell^2\sin\phi\tan\phi}{k_\phi}}, \tag{90}$$

$$\nu_{32} = -\frac{d\epsilon_2}{d\epsilon_3} = -\frac{X_3}{X_2}\frac{\frac{\sin\theta\sin\phi}{k_\ell} - \frac{\ell^2\sin\theta\sin\phi}{k_\phi}}{\frac{\cos\phi}{k_\ell} + \frac{\ell^2\sin\phi\tan\phi}{k_\phi}}. \tag{91}$$

Auxetic behaviour

The separate phenomena that can instigate auxetic behaviour are as follows:

1. *Re-entrancy*: Re-entrant angles combined with rotation within a material's microstructure as seen in the bow-tie model in Refs. [18, 26, 29]. Unfurling and unrolling of membranes are included here.
2. *Interaction ratio*: A microstructure comprising of discrete, interacting units as seen in Bathurst and Rothenburg [10] and Koenders and Gaspar [22] whereby the normal interaction is weaker than the tangential interaction.
3. *Heterogeneity*: A material that has a large degree of heterogeneity may display auxetic behaviour. The heterogeneity may be of discrete parameters such as rib angles or continuous parameters such as elastic stiffnes. See, for example, Gaspar et al. [15] and Milton [27]. This is not considered in this work, especially as the model is of a unit cell in a uniform medium.
4. *Phase-change*: Phase changes can induce a volume change; either positive or negative. It is a moot point whether this volume change be considered a Poisson's ratio phenomen. It is not recognised as such in this work and does not feature in the bulk of work on auxetics.

The first of these three is captured in this work by particular orientations of the fibril with respect to the nodule and the material axis. Auxetic behaviour occurs then by the bending of the fibril. The second is captured in the balance between fibril stretching and the fibril bending/hinging and enumerated by the ratios k_ℓ/k_ϕ and k_ℓ/k_θ. In this second case auxetic behaviour occurs by stretching deformation being more dominant than bending in the absence of re-entrant angles. The following section gives some realistic bounds on the interaction ratio if the fibril is a simple elastic body.

Interaction ratio

For a given material the parameters k_ℓ/k_ϕ and k_ℓ/k_θ can be measured using microtensile techniques [24]. In this case the possible range of values will be considered by treating the deforming fibril as a uniform elastic cylinder that bends and stretches. Further variability is included by allowing the elastic cylinder to be hollow or have a very weak inner core. Physically this may represent a case where the fibril is drawn forming a stiff outer sheath around a compliant core. The discussion is (quite sufficiently) kept to first-order approximation by using an engineering description rather than Timoshenko beam analysis. This elastic cylinder is length ℓ and has inner and outer diameters of d_i and d_o, respectively. The cross-sectional area and second moment of inertia are

$$A = \frac{\pi}{4}\left(d_\mathrm{o}^2 - d_\mathrm{i}^2\right), \tag{92}$$

$$I = \frac{\pi}{64}\left(d_\mathrm{o}^4 - d_\mathrm{i}^4\right). \tag{93}$$

The standard relations between force and displacement for the stretching and bending of a beam are:

$$k_\ell = \frac{f}{\delta} = \frac{AE}{\ell}, \tag{94}$$

$$k_\phi = k_\theta = \frac{f}{\delta} = \frac{3EI}{\ell^3}, \tag{95}$$

and so

$$\frac{k_\theta}{k_\ell} = \frac{3}{16}\frac{d_o^2 + d_i^2}{\ell^2}. \tag{96}$$

An approximate lower bound for k_θ/k_ℓ and k_ϕ/k_ℓ is therefore a solid, long slender beam. Representative values are:

$$d_\mathrm{i} = 0\ell, \quad d_\mathrm{o} = 0.001\ell \Rightarrow \min k_\theta/k_\ell = 1.9 \times 10^{-7}. \tag{97}$$

The upper bound would be a hollow, short stubby beam with the following representative values:

$$d_\mathrm{i} = 0.9\ell, \quad d_\mathrm{o} = 1\ell \Rightarrow \max k_\theta/k_\ell = 3.4 \times 10^{-1}. \tag{98}$$

The interaction ratio is essentially in opposition to the first phenomenon. Broadly speaking a geometric and mechanical environment that produces auxetic behaviour through bending beam/re-entrancy will inhibit auxetic behaviour through a stiff interaction ratio, and vice versa. This is examined in more detail by considering the ranges for which the Poisson's ratio is negative in the various planes for combined deformation. For a single deformation mechanism this has already been addressed by Figs. 3, 5 and 6.

Re-entrant angles

Consider then the faces of the material that display re-entrancy as the material properties θ and ϕ are varied. For any particular combination of θ and ϕ, there may be zero or two faces that show re-entrant angles. There may also be "inverted" angles where a fibril or its projection in a face sits over the nodule. Inverted angles have the same effect on the Poisson's ratio as non re-entrant angles. Figure 9 displays the four variations and Figs. 10 and 11 show the corresponding Poisson's ratios for varying values of $k = k_\theta/k_\ell = k_\phi/k_\ell$.

With the idealised deformation, the transition from positive to negative Poisson's ratio is dominated by geometric angles and therefore takes place conveniently at integer multiples of $\frac{\pi}{2}$ in θ and ϕ. However, when combined deformation is allowed the location in θ and ϕ of the transition from positive to negative varies. More specifically they are a function of the mechanical parameters k_θ/k_ℓ and k_ϕ/k_ℓ and also ϕ. Figures 10 and 11 show the varying values of v cases of Fig. 9. It can be seen that there are two conditions for the Poisson's ratio to change sign. From Eqs. 86–91 the points can be evaluated: firstly $v_{21} = 0$ and $v_{12} = 0$ for the same condition when

$$\frac{k_\phi}{k_\ell} = \frac{\ell^2 \cos\phi \cot\phi k_\theta}{\ell^2 k_\ell - \sin\phi}, \tag{99}$$

and the remaining Poisson's ratio changes sign when

$$\frac{k_\phi}{k_\ell} = \ell^2. \tag{100}$$

Fitted data for combined deformation

The goal here is to fit the entire 3D behaviour of the model to measured data. If only one set of axis is fitted at a time then naturally a better fit is acquired but at the expense of not representing the material response in other axis. With this 3D model, obtaining fitting parameters in two axes automatically constrain the third and so predictions of a material's property can be made in an axis that cannot be measured.

Caddock and Evans [12] have previously measured the strain dependent Poisson's ratio of expanded PTFE of

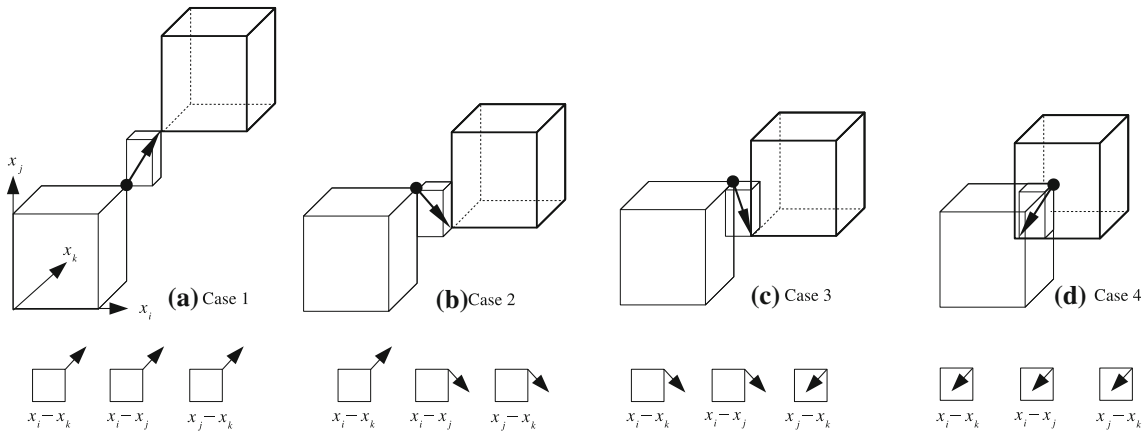

Fig. 9 The four different cases for re-entrant angles and their projections on the three orthogonal face. *Case 1* no re-entrant angles, *Case 2* 2 re-entrant angle, *Case 3* 2 re-entrant angles and 1 inverted angle, *Case 4* 3 inverted angles

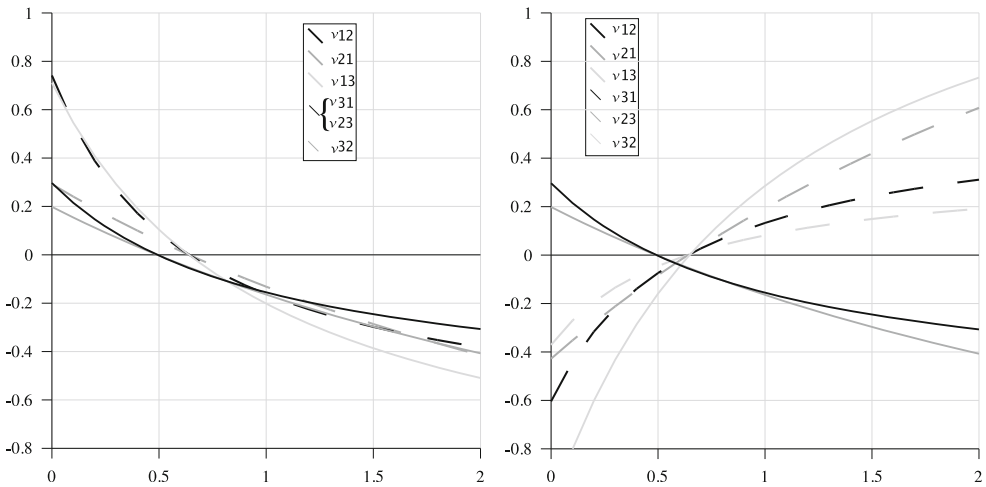

Fig. 10 ν against $k_\theta/k_\ell = 0.8$ $\times k_\phi/k_\ell = k$ for Case 1: $\theta = \frac{\pi}{6}$, $\phi = \frac{\pi}{4}$ (*left*), and case 2: $\theta = \frac{\pi}{6}$, $\phi = \frac{3\pi}{4}$ (*right*)

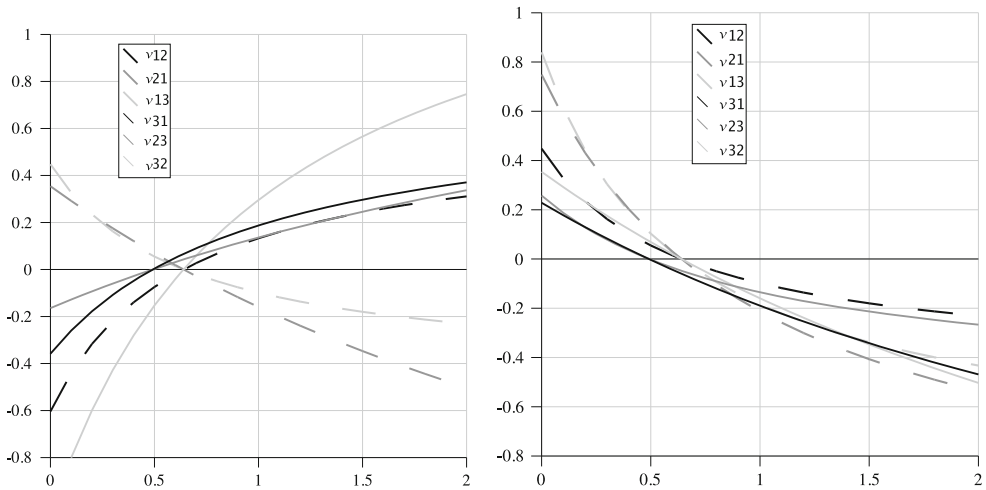

Fig. 11 ν against $k = k_\theta/k_\ell = k_\phi/k_\ell$ for Case 3: $\theta = -\frac{\pi}{6}$, $\phi = \frac{3\pi}{4}$ (*left*), and Case 4: $\theta = -\frac{4\pi}{6}$, $\phi = \frac{3\pi}{4}$ (*right*)

sections of cylindrical arterial prothesis. Their results for the Poisson's ratios v_{zr}, $v_{z\theta}$, $v_{\theta\ r}$, $v_{\theta\ z}$ show a complex and strain-dependant behaviour across the three axis. Their micrographs demonstrate a microstructure that is a candidate for this generalised 3D model. Therefore, values for the model parameters a, b, c, ℓ, θ, ϕ, k_θ/k_ℓ, k_ϕ/k_ℓ have been sought that best fit the measured data and are shown in Table 1. The four Poisson's ratios reported by Caddock

Table 1 Best fit parameters for this model to measured data by Caddock and Evans [12]

a	b	c	ℓ	θ	ϕ	k_θ/k_ℓ	k_ϕ/k_ℓ
3	4	4	1	35	100	0.05	0.01

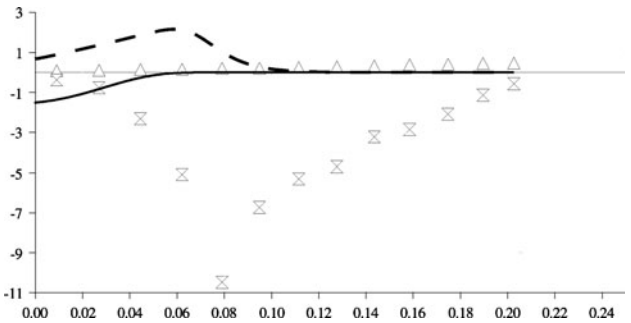

Fig. 12 Comparison of fitted curves to measured values for the incremental Poisson's ratio as a function of true strain ε_z (v_{zr}—*solid line* and *cross*, $v_{z\theta}$—*dashed line* and *open triangle*

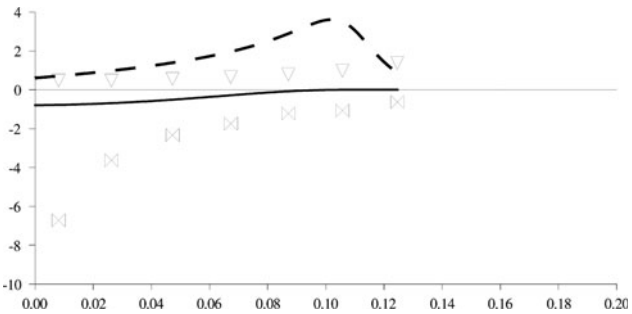

Fig. 13 Comparison of fitted curves to measured values for the incremental Poisson's ratio as a function of true strain ε_θ ($v_{\theta r}$—*solid line* and *cross*, $v_{\theta z}$—*dashed line* and *open triangle*

and Evans are all for a single set of data so it has been attempted to fit all of their data to a single set of parameters for the combined deformation of this model. The original data and this fitted model are reported in Figs. 12 and 13. It should be noted that in this case the Poisson's ratio is the incremental response and numerical techniques have been used to calculate the strain path of this model. A cursory glance suggests a poor fit, however, the model is able to match the *sign* of measured data simultaneously across the reported axis and strain path. That is in Figs. 12 and 13 the experimentally measured incremental Poisson's ratios all take the same sign as those predicted by this model even if their values are quite wrong. Attention is drawn to the fact that in all three planes the Poisson's ratio is correctly matched to be positive or negative simultaneously reflecting the 3D nature of the Poisson's ratio within the material.

An advantage of this theoretical model is now evident. Whereas only four of the possible six Poisson's ratio were

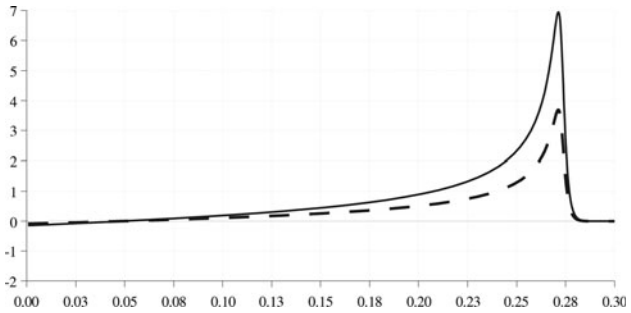

Fig. 14 Predicted values for v_{rz} (*solid line*) and $v_{r\theta}$ (*dashed line*) against true strain ε_r

measured by Caddock and Evans the fitted model parameters specify the entire 3D model and therefore the last two can be predicted. This is shown in Fig. 14.

Conclusions

Regions of auxetic behaviour

The idealised deformation model shows clear geometric regions where auxetic behaviour is obtained with sharply defined boundaries between them. There are two regions where auxetic behaviour can be obtained in all faces simultaneously. When a more realistic combined deformation model is implemented then a more complex parameter space is obtained. Notably, auxetic behaviour is dominated by the bending of beams in re-entrant angles which limits the number of planes in which auxetic behaviour can be formed. Fully auxetic behaviour can not be obtained through re-entrancy within a regular material: allowing disorder would avoid this limitation. This highlights the weakness of, for example, models of auxetic foams that rely on a regular unit cell.

To obtain fully auxetic behaviour (i.e. $v_{ij} < 0$ in all planes) then the interaction ratio has to be made large, dominating re-entrant angles and effectively returning to the idealised deformation model. The approximate upper bound in Eq. 98 (3.4×10^{-1}) is much less than the value of k in Figs. 10(Case 1) and 11(Case 4), for which $v_{ij} < 0$. This, therefore, suggests that it would be difficult to make a fibril structure with sufficiently large interaction ratio to induce auxetic behaviour—plausibly one could form arrays of fibrils that act together to fix angles such as piston models.

Data fitting

Fitting the idealised models to measured data (Fig. 8) in a single plane produces very poor fits. Great improvements are made by using the concurrent deformation models.

Since they have more parameters a better fit is expected, however, the importance of this model is to capture behaviour in all three dimensions. Therefore, the concurrent deformation model is fitted to measurements in more than one plane simultaneously. Results in Figs. 12 and 13 are not immediately impressive, however, two important points are noted. Firstly the *sign* of the Poisson's ratio is captured, so the existence of auxetic behaviour can be captured, and secondly the behaviour of the third axis can be predicted from the first two. This is a significant extension to previous models that simplify or constrain real materials to 2D behaviour.

Acknowledgement The authors acknowledge Brian Caddock of Liverpool University for his contribution to the model at the inital stages of this work.

References

1. Alderson A, Alderson K, Evans K, Grima J, Williams M, Davies P (2005) Phys Status Solidi B 242(3):499
2. Alderson A, Evans K (1995) J Mater Sci 30(13):3319. doi: 10.1007/BF00349875
3. Alderson K, Webber R, Evans K (2007) Phys Status Solidi B 244(3):828
4. Alderson KL, Alderson A, Evans KE (1997) J Strain Anal Eng Des 32(3):201
5. Alderson KL, Evans, KE (1993) J Mater Sci 28:4092. doi: 10.1007/BF00351238
6. Alderson KL, Evans KE (1994) Acta Metall Mater 42:2261
7. Alderson KL, Fitzgerald A, Evans KE (2000) J Mater Sci 35:4039. doi:10.1023/A:1004830103411
8. Badawi K, Goudeau P, Durand N (1998) Eur Phys J Appl Phys 2(1):1
9. Bathurst RJ, Rothenburg L (1988) J Appl Mech 55(1):17
10. Bathurst RJ, Rothenburg L (1988) Int J Eng Sci 26(4):373
11. Bowick MJ, Travesset A (2001) Phys Rep 344(4–6):255
12. Caddock B, Evans KE (1995) Biomaterials 16:1109
13. Evans KE, Nkansah MA, Hutchinson IJ, Rogers SC (1991) Nature 353(6340):124
14. Gaspar N, Koenders MA (2001) J Eng Mech 127(10):987 (Special Issue of the ASCE Journal of Engineering Mechanics on Statics and Flow of Dense Granular Systems)
15. Gaspar N, Ren X, Smith C, Grima J, Evans K (2003) Acta Mater 53(8):6143
16. Gaspar N, Smith CW, Behne E, Seidler GT, Evans KE (2005) Phys Status Solidi B 242(3):550
17. Gaspar N (2010) Mech Mater 42:673
18. Gibson LJ, Ashby MF, Schajer GS, Robertson CI (1982) Proc R Soc Lond A 382:25
19. Gibson LJ, Ashby MF (1997) Cellular solids: structure and properties, 2nd edn. Cambridge University Press, Cambridge
20. Grima J, Alderson A, Evans K (2005) Phys Status Solidi B 242:561
21. Grima J, Jackson R, Alderson A, Evans K (2000) Adv Mater 12(24):1912
22. Koenders MA, Gaspar N (2008) Phys Status Solidi B 245(3):539
23. Lakes R (1987) Science 235:1038
24. Lethbridge Z, Williams J, Walton R, Smith C, Hooper R, Evans K (2006) Acta Mater 54(9):2533
25. Love AEH (1927) The mathematical theory of elasticity, 4th edn. Cambridge University Press, Cambridge
26. Masters IG, Evans KE (1996) Compos Struct 35(4):403
27. Milton GW (1992) J Mech Phys Solids 40(5):1105
28. Smith C, Wootton R, Evans K (99) Exp Mech 39(4):356
29. Smith CW, Grima JN, Evans KE (2000) Acta Mater 48(17):4349
30. Smith FC, Scarpa F, Chambers B (2000) IEEE Microw Guided Lett 10(11):451
31. Zhu HX, Knott JF, Mills NJ (1997) J Mech Phys Solids 45(3):319